Secondary Atomization Characteristics of Biofuels with Different Physical Properties

P. X. Pham, A. Kourmatzis, and A. R. Masri

Clean Combustion Research Group

School of Aerospace, Mechanical and Mechatronic Engineering

The University of Sydney, NSW 2006, Australia

Abstract

A novel processing technique developed previously has now been automated and extended so that the complex shapes of fluid elements that dominate the secondary atomization process of mono-dispersed droplets in a constant velocity cross flow are classified and quantified. The experiments are conducted using high speed microscopic backlit imaging along with a calibrated image processing code, in conjunction with Laser Doppler Anemometry/Phase Doppler Anemometry (LDA/PDA) where applicable. Diesel, ethanol and a broad range of biodiesels with different flow-ability properties are investigated under a range of Weber numbers corresponding to bag, multi-mode, sheet stripping, and catastrophic breakup regimes. Using the parent droplet diameter and the object aspect ratio, the liquid filaments are classified into small spherical drops, larger objects and ligaments. It is found that at lower Weber numbers ($We<100$), fuel type influences the total breakup as reflected by the probability of detecting each of the three fragment types. The distinction is less clear at higher We where the probabilities for detecting various fluid shapes are similar for all fuels used here.

Introduction

Liquid fuel atomization encompasses a number of phenomena including primary atomization and secondary breakup. In the primary zone, instabilities on the fluid surface initiate the process where the bulk liquid breaks up to form ligaments of various shapes [1]. Aerodynamic forces will then cause these shapes to break up further in the secondary zone forming smaller droplets and other fragments [1-6]. Break-up is generally achieved by liquid-air interfacial aerodynamic forces which can be enhanced by surrounding gas phase turbulence. This paper aims to examine secondary atomization characteristics for a broad range of biodiesels as well as ethanol and fossil diesel. The configuration selected is a simple liquid jet in cross flow air stream. The range of physical properties covered in the fuels selected is sufficiently broad to enable a comparison of biodiesel from various feed stocks with neat diesel.

The fundamentals of secondary atomization mechanisms have been investigated extensively over the last two decades [1-6] and a comprehensive review of this topic can be found in [7]. The effects of liquid properties such as viscosity and surface tension are accounted for by using the non-dimensional parameters such as the Reynolds number (Re), liquid jet Ohnesorge number (Oh) and the drop Weber number (We) all of which are used to generate regime diagrams that characterise the various modes of secondary atomization [1-6]. Calculations for the non-dimensional parameters are provided in Equations 1 to 3. The literature on secondary atomization [7] refers to three research approaches using (i) shock tube methods, (ii) cross flow air streams, and (iii) drop towers. The cross flow air stream which involves droplets falling freely perpendicular to an air stream is employed in this thesis due to its simplicity and ease of experimentation. Two fundamental requirements must be satisfied: (i) a low initial drop velocity such that no breakup occurs outside the air jet and (ii) the droplets' traveling time to pass the boundary layer must be less than the initial breakup time [7].

$$\mathrm{Re} = \frac{\rho_g . U_g . d_o}{\mu_g} \qquad (1)$$

$$Oh = \frac{\mu_l}{\sqrt{\rho_l . \sigma_l . d_o}} \qquad (2)$$

$$We = \frac{\rho_g . U_r^2 . d_o}{\sigma_l} \qquad (3)$$

where ρ_l is the liquid density; ρ_g is the gas density; U_r is the relative velocity; U_g is the gas velocity; d_o is the droplet diameter; μ_g is the gas dynamic viscosity; μ_l is the liquid dynamic viscosity; and σ_l is the liquid surface tension.

Measurement techniques in non-dilute sprays remain limited with shadowgraph methods still being the most commonly used, second to PDA which is restricted to spherical droplets (with a size range from 2-120 um in the LDA/PDA system used in this study). A key limitation of shadowgraph imaging is that it provides line-integrated images that require careful calibration for the accurate quantification of de-focused objects [8]. To deal with the de-focusing problem, background thresholds for binarization must be determined as suggested by Yule et al. [9] and extended by Kashdan et al. [8, 10] with a multi-thresholding algorithm recently introduced by Ju et al. [11]. Calibration of the present image processing technique can be found in [21]. Backlit imaging has been used to observe a number of phenomena including observation of breakup morphology [12], the deformation rate of drops [13] and the qualitative evolution of ligaments [14]. The technique is also employed to observe and estimate the Rayleigh-Taylor and Kelvin-Helmholtz instability wavelengths [15-17]. To distinguish different filament types, a number of shape quantifying parameters has been reviewed extensively in [18] in which the two most common parameters are the ratio of area over the square of perimeter of the object and the aspect ratio, respectively. Despite these advances, the characterization of fluid elements that arise from secondary atomisation remains vague and this paper attempts to provide a methodical approach to this characterization which, in turn, allows for a better physical understanding of the secondary atomization process.

A technique for processing shadowgraph images has recently been developed by Kourmatzis et al. [19] and applied to the classification of different types of fluid elements. The technique

has now been automated and is extensively used in this report. The categorization developed by Kourmatzis et al. [19] has been generalized further here for simplicity (see Section 3.2) to investigate the probability of occurrence of a range of common fluid elements (here referred to as: small drops, ligaments and irregular fragments) during the secondary atomization process. Mono-droplets of ethanol, diesel, and a broad range of biodiesels are studied as a function of initial conditions. Such characterization of the complex liquid structures would be extremely useful in the development of representative models for secondary atomization processes.

Experimental setup

An air cross flow system, shown schematically in Figure 1 consists of compressed air supplied to a mini-tunnel which contains the final air discharge nozzle at its exit. Upstream of the nozzle, a number of laminarizing grids are inserted to eliminate flow instability at the exit plane. Mono-dispersed droplets were generated and delivered vertically to the cross flow using a syringe pump and a needle with an internal diameter ID = 210 um. The injection rate is kept constant at 150 ml/h. The mean diameter of the mono-dispersed droplets was measured using a long distance microscope lens providing an initial diameter equal to 400 um ($\pm$5%) independent of the tested liquids. The observation reveals that droplet generation process is driven by a Rayleigh dripping regime where the droplet diameter d = 1.89*ID [20]. Six fuels are selected here including ethanol (E), fossil diesel (D) and four different biodiesels (B1 to B4). Selected properties for these fuels are listed in Table 2 and more details of these fuels have already appeared elsewhere [21-23].
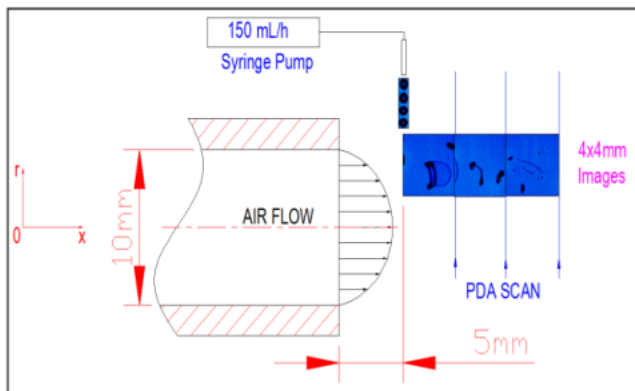

Figure 1. Schematic of the cross-flow experimental system

It should be noted that an initial droplet breakup location has been observed (from the shadowgraph images) at radial location of r/D~0.4. This location is identified where the primary droplets start changing their vertical trajectory and deforming and remains consistent regardless of the fuel types and air velocity conditions. Using flow conditions (velocity) at the initial breakup point, local Weber and Reynolds numbers are computed and used to describe the breakup regimes. At this initial breakup point, the horizontal liquid drops' velocity is approximately zero and can be ignored. The relative velocity (U_r), therefore, is equal to the gas velocity (U_g) which is measured using an LDA system similar to that used in [19]. The air flow rate is adjustable to achieve a range of local droplet Weber numbers from 20 to 400 covering bag, multi-mode, sheet stripping, and catastrophic breakup regimes. The same local Weber numbers are used amongst the fuels and these are controlled based on the local air velocity at the initial breakup location of the droplets. The test conditions are listed in Table 1.

A full description of the microscopic shadowgraph imaging system and LDA/PDA setup can be found in [19, 21]. The high speed camera (LaVISION, CMOS) was used in conjunction with a long distance microscope objective lens (QUESTAR, QM-100) in order to visualize a scale of 4x4 mm with a 512x512 pixel resolution. A diode stack Nd-YAG laser operated at 532 nm and 5 kHz was used as the high speed light source (Edgewave INNOSLAB model HD3011E) with an average power of 10 W corresponding to 2mJ/pulse. Two opal glass diffusing optics were used to remove laser coherence in order to provide a uniform source of illumination. A sequence of 1,000 consecutive images is recorded for each atomization condition and three downstream locations corresponding with x/D = 0.9, 1.3 and 1.7 are investigated (see Figure 1). It has been shown in our previous work [19] that 100 images could be sufficient to generate reliable statistics for the shape populations.

Table 1. Breakup regimes and conditions (Local We numbers are the same amongst the tested fuels; minimum Re and Oh numbers in each regime are for E, the lowest viscosity fuel, while maximum values are for B4, the highest viscosity fuel)

Breakup Regime	Bag	Bag	Multi-mode	Sheet Stripping	Catastrophic
Local We	20	45	95	245	400
Local Re	700-950	1,050-1,400	1,520-2,050	2,480-3,300	3,100-4,200
Oh	0.018-0.047	0.018-0.047	0.018-0.047	0.018-0.047	0.018-0.047

Table 2. Selected physical properties of the tested fuels

Fuel	**B1**	**B2**	**B3**	**B4**	**E**	**D**
Density, [kg/m3]	877	871	873	879	789	848
Viscosity, [Pa.s]*10^{-3}	1.71	3.81	4.32	4.65	1.3	3.2
Surface tension, [N/m] *10^{-3}	25	33	44	28	22	26

Results
Breakup Morphology

Using the backlit technique described in Section 2, breakup morphology of the droplets was observed for all tested fuels at different Weber numbers (We = 20, 45, 95, 245 and 400). Differences in the secondary atomization of different fuels are expected as the break-up time is a function of surface tension and viscosity [1] which vary from fuel to fuel. However, the break-up patterns observed for the various fuels are somewhat similar and hence representative images are shown here for one fuel only. Figure 2 shows image samples of the breakup morphology for fuel B3 and range of We numbers. The increased fragmentation with increasing We is evident from this figure. A statistical technique, which is needed to describe a quantifiable characterization of secondary atomization for these fuels, will be described in the flowing section.

Object Classification

Complex liquid fragments observed from the secondary atomization process are classified into: small drops, large objects and ligaments. The imaging technique monitors the centroid of object and the characteristic length of the major and minor axes. Using diameter of the parent droplets (d_o) as a reference, the fragments are classified into three categories as shown in Table 3. The ratio of major to minor axis (d_{max}/d_{min}) is also known as aspect ratio (AR). A small drop is an object with its major axis length (d_{max}) is lower than d_o and an AR < 3. A large object has a $d_{max} > d_o$ and an AR < 3. Ligaments are fragments with AR > 3. It can be seen from this study that, further downstream, the small

drops do not continue breaking up while, in contrast, the large objects and ligaments continue to generate ligaments and small droplets.
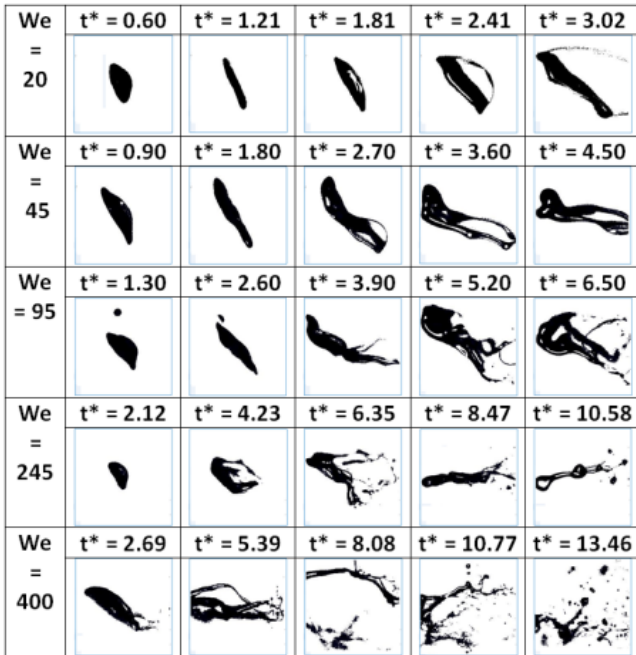

Figure 2. Droplet morphology of Biodiesel B3 at x/D = 0.9; We = 20, 45, 95, 245 and 400; shown as a function of the relaxation time (normalized resident time by characteristic breakup time [1]) where the field of view is cropped to 2.7x2.7mm

Table 3. Liquid fragment classification (d_{max} and d_{min}: major and minor axis, respectively; AR = d_{max}/d_{min})

Small drops	Large objects	Ligaments
$d_{max} < d_o$ and AR < 3	$d_{max} > d_o$ and AR < 3	AR > 3

Probability

The probability of occurrence of the classified droplet shapes described earlier in Section 3.2 is determined for the various fuels studied here over a range of conditions. The overall probability is calculated simply as the total number of a particular shape counted, normalized by the total number of all objects counted over all images. The results are presented in the form of probabilities plotted versus axial distance from the point of injection as shown in Figure 3 where the probability of small drops (Figure 3a), large objects (Figure 3b), and ligaments (Figure 3c) are presented for a range of fuels at We = 245.

It is interesting to note that when comparing the six fuels listed in Table 2, the probability of ligaments (Figures 3c) is very similar regardless of the fuel properties. However, low viscosity fuels (E, B1 and B2) show differences in their probability of small drops and large objects with respect to their high viscosity counterparts (B3, B4 and D). Upstream, the small droplet probability of E and B1 is approximately 10 to 20% higher than those of the high viscosity fuels. This indicates that closer to the initial break-up

location there is a higher propensity to form droplets for lower viscosity liquids and this coincides with a lower probability of detecting larger objects for the lower viscosity fuels. The difference in the probability of small drops remains until x/D = 1.3 where the probability of low viscosity fuels fluctuates around 0.8 downstream while the probability of higher viscous fuels continue increasing. At x/D = 1.7, the probabilities of all fragments are almost similar to all the tested fuels. This implies that the total liquid breakup time depends on the physical properties. At a certain downstream location, when the breakup has occurred, the generated liquid fragment population is similar regardless the fuel types.

Figure 4 shows the probability for the classified fragments now plotted versus Weber number. These values are shown at the furthest axial location x/D = 1.7 where break-up has occurred for all cases.
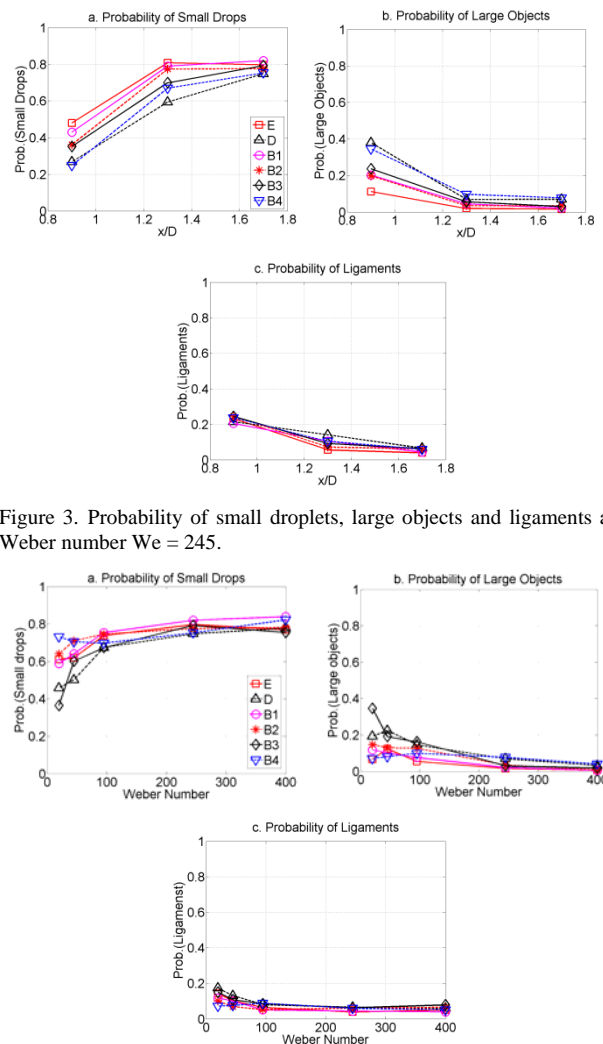

Figure 3. Probability of small droplets, large objects and ligaments at a Weber number We = 245.

Figure 4. Probability of small droplets, large objects and ligaments at x/D = 1.7 for a range of Weber numbers.

Under the bag breakup regime (We < 100), a very steep increase in small drop probability is observed, while reductions in probability are observable for all other objects. When We increases past 100, only a slight increase in the small droplet probability is noted (Figure 4a) and this coincides with a slight decrease in the probabilities of large objects (Figure 4b) as well as ligaments (Figure 4c). Similar to what has been observed in

3

Figure 3, fuels E and B1 usually show a higher probability for small drops but lower probability for large objects when compared with other fuels. The results presented thus far suggest that the morphological characteristics of all fuels are quite similar at high Weber numbers and when traversing further downstream. However, in the bag break-up regime, there are significant differences that are not necessarily consistent with the physical properties of the fuels. For example, fuel B4 is shown to have a larger population of small drops than E. This inconsistency may be partly attributed to the larger variation amongst break-up events when in low Weber number bag break-up regimes. This can in part be due to a slight variation in the local velocity which can expose each droplet to a slightly different instantaneous Weber number. While this is not ideal, it is to be expected given the slight turbulence intensity.

This further confirms the importance of carrying out statistical analysis on these images rather than treating only single representative snapshots without local flow field measurements. The similarity in the probability of object detection amongst fuels at higher Weber numbers agrees with previous findings in Kourmatzis et al. [19] for a coaxial airblast atomizer using a manual technique. In addition, it is clear that over a Weber number of approximately 200, there is a negligible difference in the change in probability of a particular object shape. This demonstrates that once a threshold Weber number is achieved, differences in the probability of occurrence of particular shapes from We = 200 to 400 (which represent more than one break-up regime) are insignificant. This is true despite the fact that the initial break-up morphology may look qualitatively different in a selection of images. This has implications in the modelling of droplet break-up, particularly using Eulerian methods. This suggests that analysis of the probability of detecting particular shapes is only necessary for lower Weber numbers. While there is a level of uncertainty in these measurements as detailed and quantified in [19, 21], there are clearly consistent trends in the results which therefore do merit further investigation.

Conclusion

The morphological characteristics of complex liquid filament shapes formed after the secondary breakup of mono-dispersed droplets of four well defined biodiesels, fossil diesel and ethanol in a cross-flow air stream have been investigated extensively using microscopic backlit imaging and LDA/PDA. The images have been processed using an automated imaging code which computes the probability of three pre-classified filament shapes (small drops, large objects, and ligaments). Characterization of the spray formed from secondary atomization shows that the mono-dispersed droplet stream enters the air jet in an area of low turbulence intensity. Computation of the probability of detection of particular liquid fragment shapes shows how objects undergo a conversion from ligaments to small droplets as they traverse downstream after secondary break-up providing detailed quantitative information on the breakup zone. A significant change in shape probabilities occurs when moving from a bag break-up regime to higher Weber numbers. However, above a We = 200 there is little difference in the probability of detection of different shapes, suggesting that even though the break-up regimes are different, this particular statistic is unchanged.

Acknowledgements

References

[1] Hsiang L. P. & Faeth G. M., Near-limit drop deformation and secondary breakup, Int. J. Multiphase Flow, 18, 1992, 635-652.

[2] Lane W. R., Shatter of drops in streams of air, Industrial Engineering Chemistry, 43, 1951, 1312-1317.

[3] Hinze J. O., Fundamentals of the hydrodynamic mechanism of splitting in dispersion processes, AIChE, 1, 1955, 289-295.

[4] Hanson A. R., Domich E. G. & Adams H. S., Shock tube investigation of the breakup of drops by air blasts, Phys. Fluids, 6, 1963, 1070-1080.

[5] Loparev V. P., Experimental investigation of the atomization of drops of liquid under conditions of a gradual rise in the external forces, Fluid Dynamics, 10, 1975, 518-521.

[6] Krzeczkowski S. A., Measurement of liquid droplet disintegration mechanisms, International Journal of Multiphase Flow, 6, 1980, 227-239.

[7] Guildenbecher D. R., Lopez-Rivera C. & Sojka P. E., Secondary atomization, Exp. In Fluids, 46, 2009, 371-402.

[8] Kashdan J. T., Shrimpton J. S. & Whybrew A., Two-phase flow characterization by automated digital image analysis. Part 1: Fundamental principles and calibration of the technique, Part. Part. Syst. Charact, 20, 2003, 387-397.

[9] Yule A. J., Chigier N. A. & Cox N., Measurement of particle sizes in sprays by the automated analysis of spark photographs, Particle Size Analysis N/A, 1978, 61-73.

[10] Kashdan J. T., Shrimpton J. S., and Whybrew A., Two-phase flow characterization by automated digital image analysis. Part 2: Application of PDIA for sizing sprays, Part. Part. Syst. Charact., 21, 2004, 15-23.

[11] Ju D., Shrimpton J. S. & Hearn A., A multi-threshold algorism for sizing out of focus particles, Part. Part. Syst. Charact., 29, 2012, 78-92.

[12] Arcoumanis C., Khezzar L., Whitelaw D. S. & Warren B. C. H., Breakup of Newtonian and non-Newtonian fluids in air jets, Experiments in Fluids, 17, 1994, 405-414.

[13] Park S. W., Kim S., & Lee C. S., Effects of mixing ratio of biodiesel on breakup mechanisms of monodispersed droplets, Energy and Fuels, 20, 2006, 1709-1715.

[14] Arcoumanis C., Whitelaw D. S. & Whitelaw J. H., Breakup of droplets of Newtonian and non-Newtonian fluids, Atomization and Sprays, 6, 1996, 245-256.

[15] Varga C. M., Lashera J. C. & Hopfinger E. J., Initial breakup of a small diameter liquid jet by a high-speed gas stream, J. Fluid Mech., 497, 2003, 405-435.

[16] Liu A. B. & Reitz R. D., Mechanism of air-assisted liquid atomization, Atomization and Sprays, 3, 1993, 55-75.

[17] Hwang S., Liu Z. & Reitz R. D., Breakup mechanism and drag coefficients of height-speed vaporizing liquid drops, Atomization and Sprays, 6, 1996, 353-376.

[18] Ghaemi S., Rahimi P. & Nobes D. S., Assessment of parameter for distinguishing droplet shape in a spray field using image-based technique, Atomization and Sprays, 19, 2009, 809-831.

[19] Kourmatzis A., Pham P. X. & Masri A. R., Air assisted atomization and spray density characterization of ethanol and a range of biodiesels, Fuel, 108, 2013, 758-770.

[20] Lefebvre A. H., Atomization and Sprays, Taylor & Francis, 1988.

[21] Pham P. X., Influences of molecular profiles of biodiesel on atomization, combustion and emission characteristics, thesis submitted in fulfilment of the requirements for the degree of Doctor of Philosophy, The University of Sydney, 2014.

[22] Pham P., Bodisco T., Stevanovic S., Rahman M., Wang H., Ristovski Z., Brown R. & Masri A., Engine performance characteristics for biodiesels of different degrees of saturation and carbon chain lengths, SAE Int. J. Fuels Lubr., 6, 2013, 188-198.

[23] Pham P. X., Bodisco T. A., Ristovski Z. D., Brown R. J. & Masri A. R., The influence of fatty acid methyl ester profiles on inter-cycle variability in a heavy duty compression ignition engine, Fuel, 116, 2014, 140-150.

[24] Nicholls J. A. & Ranger A. A., Aerodynamic shattering of liquid drops. AIAA Journal, 7, 1969, 285-290.

[25] Taylor G., The instability of liquid surfaces when accelerated in a direction perpendicular to their planes. , Proceedings of the Royal Society Lond., 201, 1950, 191-196.